

Repository Istituzionale dei Prodotti della Ricerca del Politecnico di Bari

Non-linear finite element prediction of the performance of a deep excavation in Boston Blue Clay

This is a post print of the following article

Original Citation:
Non-linear finite element prediction of the performance of a deep excavation in Boston Blue Clay / Rouainia, M., Elia, G., Panayides, S., Scott, P.. - In: JOURNAL OF GEOTECHNICAL AND GEOENVIRONMENTAL ENGINEERING. - ISSN 1090-0241. - 143:5(2017). [10.1061/(ASCE)GT.1943-5606.0001650]

Availability:
This version is available at http://hdl.handle.net/11589/102590 since: 2021-03-02

Published version
DOI:10.1061/(ASCE)GT.1943-5606.0001650

Publisher:

Terms of use:

(Article begins on next page)

17 November 2026

From: em.jrngteng.0.4e0165.099689e5@editorialmanager.com on behalf of Journal of Geotech. and Geoenvironmental Eng <em@editorialmanager.com>
Sent: Tuesday, September 20, 2016 5:16 PM
To: Gaetano Elia
Subject: Decision on Manuscript MS GTENG-4896R3 - [EMID:3330b4fd37a6bd8d]

Follow Up Flag: Follow up
Flag Status: Flagged

CC: mohamed.rouainia@ncl.ac.uk, stelios.panayides@subsea7.com, peter.scott@burohappold.co.uk

Ref.: Ms. No. GTENG-4896R3
Non-linear finite element prediction of the performance of a deep excavation in Boston Blue Clay
Mohamed Rouainia, Ph.D.; Gaetano Elia, Ph.D.; Stylianos Panayides, Ph.D.; Peter Scott, M. ASCE

Dear Dr. Elia,

Your Technical Paper, listed above, has been accepted for publication in ASCE's Journal of Geotechnical and Geoenvironmental Engineering.

Your manuscript will now be forwarded to a Production Editor who will prepare it for publication. You will be notified of a publication date once your paper has been schedule for an issue.

Finally, our editors have requested that authors of accepted manuscripts serve as reviewers for Journal of Geotechnical and Geoenvironmental Engineering. If you are willing to serve as a reviewer, please reply to this email and let me know.

Thank you for submitting your work to ASCE's Journal of Geotechnical and Geoenvironmental Engineering.

Sincerely,

Jennifer Chapman
Editorial Coordinator

Title:

Non-linear finite element prediction of the performance of a deep excavation in Boston Blue Clay

Authors:

Mohamed Rouainia[1], Gaetano Elia[2], Stylianos Panayides[3], Peter Scott[4]

[1]Reader in Computational Geomechanics (Ph.D.), School of Civil Engineering & Geosciences, Newcastle University, NE1 7RU - Newcastle Upon Tyne, UK.
E-mail: mohamed.rouainia@ncl.ac.uk

[2]Lecturer in Geotechnical Engineering (Ph.D.), School of Civil Engineering & Geosciences, Newcastle University, NE1 7RU - Newcastle Upon Tyne, UK (corresponding author).
E-mail: gaetano.elia@ncl.ac.uk. Phone: +44 (0)191 2227934. Fax: +44 (0)191 2225322

[3]Geotechnical Engineer (Ph.D.), Subsea 7, East Campus, Prospect Road, Arnhall Business Park, Westhill, AB32 6FE - Aberdeenshire, UK.
E-mail: Stelios.Panayides@Subsea7.com

[4]Technical Director (M. ASCE), Buro Happold Ltd, Camden Mill, Lower Bristol Road, BA2 3DQ - Bath, UK.
E-mail: peter.scott@burohappold.co.uk

Abstract

The work investigates the behaviour of a deep excavation which forms part of a 100 m wide basement excavation located in Boston, Massachusetts, USA. Two different types of tied back retaining walls were used, i.e. a soldier pile tremie concrete wall and a traditional reinforced concrete diaphragm wall. The glacial marine clay (Boston Blue Clay) deposit was modelled with the Kinematic Hardening Model for Structured soils (KHSM), its reduced bubble model version (KHM) and the well-known Modified Cam Clay (MCC) model. The difference between the models is the prediction of softening with loss of structure as plastic strains occur. The values of the optimised soil parameters used in the simulations were obtained by a careful calibration of the models against a range of advanced laboratory and field tests performed at the site. Comparison of the available horizontal wall movements monitoring data with the undrained finite element predictions revealed a very satisfactory agreement when the KHM was used in conjunction with a small-strain elastic formulation. The relatively small increase in lateral wall deflection in the presence of initial structure accounted for in the KHSM confirms that the small-strain properties of the soil control the magnitude of excavation deformations. Finally, using a coupled-consolidation analysis and the KHSM, an excellent agreement between the observed and measured pore water pressures and ground movements of the excavation base was achieved.

CE Database subject headings:

Excavation; Constitutive models; Finite element method; Diaphragm wall; Instrumentation.

Introduction

In recent years the building engineering industry has become increasingly involved with urban environment developments. The limited availability of land for construction in both developed and developing regions of the world has seen an increase in urban regeneration projects as well as construction of various types of infrastructure such as deep basements, subways and service tunnels. For a safely and timely completion of deep excavations, the use of appropriate retaining wall and bracing systems is usually required to minimise excessive ground movements. Successful control of movements during excavation works is often as imperative as assurance against collapse. As a consequence, limiting values of deformation should be carefully prescribed in accordance to the serviceability limit state. However, excessive restrictions may well lead to uneconomic designs of deep excavations. Two techniques are commonly applied to evaluate the anticipated wall deflections and ground settlements. These involve either an interpolation from published empirical data sets (e.g. Peck, 1969; Clough and O'Rourke, 1990; Puller, 2003) or analytical and numerical methods such as finite element (FE) analyses (e.g. Chang and Duncan, 1970; Burland and Hancock, 1977; Simpson *et al*., 1979; Powrie and Batten, 2000).

Numerical methods used in conjunction with laboratory and field data are nowadays standard practice in the research community and geotechnical engineering profession. As an example, the top-down construction of a seven-storey underground parking garage at Post Office Square in Boston was modelled by Whittle *et al*. (1993) using coupled FE simulations implementing the advanced MIT-E3 model for Boston Blue Clay (BBC). Subsequently, Hashash and Whittle (1996) performed a series of non-linear FE analyses to investigate the effects of wall embedment depth, support conditions and stress-history profile on the undrained deformations around a braced diaphragm wall in a deep clay deposit. Their work provided useful design charts for the estimation of ground movements as function of the excavation depth and support conditions. Zdravkovic *et al*. (2005) modelled a deep square excavation at Moorgate station on the Crossrail route in London using the Imperial College Finite Element Program (ICFEP). The data used for the calibration of the

numerical model were based on the work by Addenbrooke *et al*. (1997), who undertook small-strain triaxial testing on samples of London Clay from the St James's Park area during the tunnelling for the Jubilee Line underground extension. Recently, Nikolinakou *et al*. (2011) studied the performance of a 20 m deep excavation in Berlin Sand using the generalised MIT-S1 model calibrated against field dynamic penetration test data, while Whittle *et al*. (2015) investigated an 18 m excavation in Boston Blue Clay required for the construction of the Silverline Courthouse Station in South Boston using the MIT-E3 model.

The paper investigates the performance of a 14.6 m deep basement excavation located in Boston using an advanced constitutive model for natural clays formulated within the framework of kinematic hardening plasticity (Rouainia and Muir Wood, 2000) and implemented as a user defined model in a FE procedure (PLAXIS 2D, 2012). The project under consideration contains valuable experimental data and provides a useful opportunity to verify the proposed FE elasto-plastic model, which in turn can be used to analyse the performance of the excavation retaining systems. The modelling framework adopted in this work entails adequate complexity and it is focused on the effects of soil constitutive assumptions on numerical predictions by starting with the well-known Modified Cam Clay model and consequently adding advanced modelling features such as stress-history dependency, anisotropy and structure.

The case study

Site location and geology

The case study investigated in this work is a 14.6 m deep, 100 m wide basement excavation above which four buildings containing up to eight storeys will form the Allston Science Complex at Harvard University in Boston, Massachusetts, USA (Buro Happold, 2007). The construction site is located off Western Avenue in Allston (Figure 1). Information on ground conditions have been collated from three site investigations. In-situ explorations included standard penetration (SPT), cone penetration (CPTU) and seismic cone penetration (SCPT) tests, self-boring pressuremeter (SBPT), and field vane testing. The location of the different in-situ investigations is reported in

Figure 1. SPT and field vane tests were undertaken in the boreholes together with associated sampling. In some of the boreholes (as indicated in Figure 1), vibrating wire piezometers were installed to determine ground water conditions with depth across the site. The groundwater table was encountered at 2.0 m below ground surface with a hydrostatic pore pressure increasing with depth. Laboratory testing consisted of K_0-consolidated undrained triaxial tests in both compression (CK_0UTC) and extension (CK_0UTE), direct shear tests (DSS), unconsolidated undrained triaxial tests, Atterberg limits, and moisture contents. The geological sequence, confirmed by the site investigations, included successive strata of made ground, alluvium deposits (occasionally including organic peat material), sandy gravel, the BBC marine clay, glacial till, and the Cambridge argillite bedrock. The identified soil profile is shown in Table 1.

The results of moisture content tests on samples of Boston Blue Clay, reported in Figure 2a, indicated values between 25% and 44%, with a slight general increase with depth. Atterberg limit tests undertaken on BBC indicated that the Plasticity Index (PI) varies between 13% and 29% with an average value of 20%; the Liquid Limit (LL) varies between 24% and 48%, and the Plastic Limit (PL) varies between 14% and 21% (Figure 2a). The Atterberg limits for the BBC plot parallel to and above the A-line. From these data, the BBC can be classified as low-plasticity clay, in line with previous research by Ladd *et al*., 1999. The combined SPT blow count (N_{SPT}) values for all layers are shown in Figure 2b. Both in-situ dissipation SBPT tests (undertaken at various depths within the two boreholes BH105 and BH106) and CRSC laboratory tests were performed to assess the permeability of the BBC layer. All the measured permeability values are shown in Figure 2c. The data from the tests indicated that the permeability values ranges between 7.60×10^{-11} m/s and 2.20×10^{-9} m/s. The results from published test data (e.g. Whittle *et al*., 1993; Whittle *et al*., 2015) and the Allston testing program exhibit good agreement, hence for design purpose a permeability value of 3.00×10^{-10} m/s, typical of clay soils, was considered. Finally, the stress history profile of the BBC deposit is summarised in Figure 2d, where the preconsolidation pressures obtained from CRSC tests and the piezometric data are also reported. According to the available geological and geotechnical data described above, the geotechnical model adopted in this study was composed first

by a 2 m thick layer of made ground (L_1), followed by a 4 m stratum of fluvial sands (L_2), and a 26 m deep BBC deposit (L_3) overlaying 8 m of glacial till (L_4) resting on the Cambridge argillite bedrock. The BBC deposit was divided in an upper overconsolidated (OC) 19 m thick layer and a lower normally consolidated (NC) 7 m thick layer.

The behaviour of the excavation is expected to be predominantly controlled by the significant thickness of the Boston Blue Clay deposit present on site. BBC is a marine deposit generally consisting of a stiff crust of lightly overconsolidated clay which becomes normally consolidated with depth. Due to its overconsolidation ratio (OCR), the potential for significant heave and movement of adjacent ground due to excavation processes exists (Ladd *et al.*, 1999). As a result, numerical modelling plays an important role in estimating ground movements associated with the excavation, and small-strain models can help to improve the accuracy of the predictions. In addition, previous laboratory investigations have indicated that the mechanical behaviour of BBC shows anisotropic stress-strain-strength, rate dependency and medium sensitivity (e.g. Santagata, 1998; Santagata and Germaine, 2002). The presence of an initial structure in the natural BBC soil has been confirmed by the results of CRSC tests performed on NC and OC samples from the Allston Science Complex (Nikolic *et al.*, 2010). Figures 3a and 3b present the CRSC loading curves, together with the intrinsic compression line (ICL) and a range of possible sedimentation compression (SC) curves. In Figure 3a the in-situ stress states for the two NC samples are also shown, which indicate a substantial agreement between the in-situ stress level and yield stress for the normally consolidated BBC. The framework developed by Cotecchia and Chandler (2000) indicates that the sedimentation compression curve for a clay deposit should be related to the particular clay sensitivity. Therefore, the use of an advanced soil constitutive model, able to describe the influence of structure and its subsequent degradation under loading, is deemed to be appropriate in this case.

Stiffness and consolidation characteristics have been determined in order to predict ground deformations resulting from the excavation. For the low level of shear strains which is expected to be induced by the excavation process, the clay has relatively high stiffness characteristics.

Additionally, laboratory tests indicate that the clay formation is characterised by very low permeability (see Figure 2c) and, as such, can be expected to behave in undrained conditions during short term construction operations. This is of considerable benefit for the temporary excavation and allows the design of a practical support structure that would otherwise be unstable. This is, however, a critical construction constraint which implies that the stability safety factors of the open excavation would decrease with time.

Excavation retaining systems

Two different types of retaining wall, a diaphragm wall (or reinforced concrete slurry wall) and a soldier pile tremie concrete (SPTC) slurry wall, were adopted for this project. The total depth of excavation was varying between 13 m and 17 m and the walls were designed to resist the soil and water pressure with four rows of tiebacks (ground anchors) at various elevations. Specifically, the reinforced concrete diaphragm wall was adopted for particular boundary sections where a significant cantilever condition was required above the top tieback level (Section A). The SPTC wall was proposed for those sections where the top tieback level was in relative proximity to the ground surface (Section B). Both manually read and automated in-place inclinometers were used in the project to measure wall horizontal movements (Chartier *et al*., 2010). The schematic plan view of the two analysed Sections A and B is reported in Figure 1, while Figure 4 shows the relevant characteristics of the two excavation support systems, in terms of tiebacks spacing, level and inclination, together with the excavation stages.

Numerical simulations

Soil constitutive models

The made ground, fluvial sand and glacial till layers were modelled using the Mohr-Coulomb (MC) soil model for which the material properties were derived from different geotechnical reports on Boston soils (i.e. Berman *et al*., 1993; Whittle *et al*., 1993; O'Rourke and O'Donnell, 1997; Ladd *et al*., 1999; Terzaghi *et al*., 1996), including the recommendations for design provided by Buro

Happold (2007). The soil properties adopted in the FE simulations for L_1, L_2 and L_4 are summarised in Table 2.

The BBC deposit was modelled with three different soil constitutive models, starting from the well-known Modified Cam Clay (MCC), followed by the hierarchical extensions of the KHM (bubble model) and the KHSM for structured soils. In addition, two different elastic assumptions were considered in this work (see Appendix A): a standard hypoelastic formulation and the small-strain stiffness equation proposed by Viggiani and Atkinson (1995). This has led to four different FE simulations of the excavation, as illustrated in Table 3. The KHSM has been formulated for natural clays within the framework of kinematic hardening with elements of bounding surface plasticity (Rouainia and Muir Wood, 2000). The model contains three surfaces (see Appendix A). The reference surface controls the state of the soil in its reconstituted, structureless form and describes the intrinsic behaviour of the clay (Burland, 1990). The outer structure surface represents the amount of current bonding in the clay. The bubble acts as the true yield surface enclosing the elastic domain of the soil, and moves around within the structure surface following a kinematic hardening rule. The centre of the structure surface can be situated off the mean effective stress axis, allowing the KHSM to accommodate the inherent anisotropy, which is a common feature of natural structured clays. The degree of structure, r, which describes the relative sizes of the structure and reference surfaces, is a monotonically decreasing function of the plastic strain thus representing the progressive degradation of the material. The KHSM has been implemented in PLAXIS 2D with an explicit stress integration algorithm adopting an automatic sub-stepping and error control scheme (Zhao *et al.*, 2005). The model has been successfully employed to simulate both static (Gonzáles *et al.*, 2012; Panayides *et al.*, 2012) and dynamic geotechnical problems (Elia and Rouainia 2013a and 2013b).

The KHSM was calibrated against CRSC, SBPT and K_0-consolidated undrained triaxial compression and extension tests performed on BBC samples from the Allston Science Complex (Nikolic *et al.*, 2010). As a result, a single set of model parameters, listed in Table 4, was derived and used to describe the mechanical behaviour of the BBC layer (L_3) in the subsequent simulations.

The compressibility parameters λ^* and κ^* were back calculated from the results of CRSC tests for the appropriate range of void ratio. The stress sensitivity approach (Burland, 1990; Cotecchia and Chandler, 2000) was adopted to quantify the initial degree of structure (i.e. r_0). Figures 5a and 5b show the comparison, in terms of volumetric strain-logarithm of vertical stress, between the KHSM predictions and two CRSC tests, one performed on an OC BBC sample and the other on a NC BBC specimen, respectively. Figure 6a depicts the stress paths normalised with respect to the preconsolidation pressure for three CK_0UTC and three CK_0UTE tests on BBC samples from the investigated site, together with the KHSM predictions. The corresponding stress-strain response is shown in Figure 6b. A critical state stress ratio (M) equal to 1.11, corresponding to a friction angle of approximately 28° during triaxial compression, was adopted. The general trend shown by the experimental results is well captured by the model in both compression and extension regimes. The model predictions are also in good agreement with the laboratory data obtained by Ladd and Varallyay (1965), Fayad (1986) and Sheahan (1991) on BBC samples from other Boston sites. In addition, the undrained secant stiffness degradation (E_u) curve obtained by Santagata *et al*. (2005) during a K_0-consolidated undrained triaxial compression test performed on a NC BBC sample under an effective vertical consolidation pressure equal to 299 kPa is shown in Figure 6c. The corresponding KHSM prediction is plotted in the same figure and shows how the general trend, in terms of stiffness degradation with increasing strain, is well captured by the model. Finally, two SBPT tests, performed at two different depths within the same borehole BH106, were simulated using the KHSM. The results are presented in Figure 7 in terms of cavity pressure response. The model is able to predict satisfactorily the stress-strain curves observed during the expansion and contraction stages of the tests.

Finite element model

Following an initial sensitivity analysis, the typical plane strain FE mesh of the cross-section A is shown in Figure 8 and consisted of approximately 2200, 15-noded triangular elements. In the analyses, which were assumed to be fully undrained, no movement was permitted at the base of the

finite element mesh and only vertical movement was allowed at the lateral boundaries. The excavation was supported by a 21 m deep retaining system, with four rows of tieback anchors. The left-hand boundary of the model was set at 150 m, which is over four times the depth of the excavation and thus is unlikely to interfere with the results (Kung *et al*., 2009). The right-hand lateral boundary represents the axis of symmetry of the analysed section. The excavation sequence for both sections consisted in the installation of the retaining wall, followed by a first excavation phase under cantilever conditions and then tiebacks installation and consecutive excavation to 0.6 m below each level of tieback. Once the last tieback was installed, the analyses simulated the final excavation to 14.6 m. During the real excavation at the Allston Science Complex, groundwater dewatering was achieved by mean of sump pumping and no drawdown of the external water level was permitted. Therefore, the water table outside the wall was kept constant at 2.0 m below ground level in the analyses. The retaining systems were modelled using plate elements, with node-to-node anchors and geogrid elastic elements adopted to simulate the tiebacks and the grout body, respectively. Material parameters for the plates include normal stiffness (EA) and flexural rigidity (EI) as given in Table 5. The geogrids' axial stiffness EA was set equal to 1.12×10^5 kN/m. The anchors, which share the same connection with the mesh nodes, were modelled as elasto-plastic elements characterised by a normal stiffness of 1.12×10^5 kN/m and a pre-stress force of 383 kN/m. Moreover, interface elements were used around the walls with a reduction strength factor of 0.67.

The K_0 profile used in the analysis was based on the design line assumed by the geotechnical report (Buro Happold, 2007) from SBPT measurements. Figure 9a shows the K_0 values used for each stratum together with published data from Berman *et al*. (1993). The four constitutive models adopted for the BBC layer were calibrated and initialised to match the same undrained shear strength (c_u) profile, which was used in the design of the excavation. This makes the FE simulations comparable to simpler total stress-based methods which are usually adopted in the design of deep excavations in clayey soils. Although c_u is not a soil property in effective stress-based constitutive models, it can be indirectly obtained by running a series of undrained triaxial compression model

simulations starting from in-situ stress conditions at several points across the entire depth of the BBC deposit with varying OCR values. The BBC undrained shear strength at the Allston Science Complex was assessed using field vane, CPTU and DSS tests. The corresponding c_u values with depth, together with the peak shear strength profile assumed in the design, are reported in Figure 9b. The shaded area represents the envelope of c_u data obtained from DSS tests. It is noted that the c_u values from the Allston project are in good agreement with the data obtained from other sites (e.g. Berman *et al*., 1993; Hashash and Whittle, 1996). The c_u profile predicted by the KHSM and its down-scaled versions (i.e. KHM and MCC) is also shown on the same figure, which closely agrees with the assumed design profile. Figure 9c shows the two OCR profiles adopted in the FE simulations to match the same in-situ undrained strength. The figure also depicts the OCR values obtained from in-situ (CPTU and SBPT) and laboratory (CRSC) tests on BBC. It can be seen that the adopted OCR profiles are in good agreement with the experimental data. Finally, the BBC small-strain shear stiffness G_0 was estimated from seismic cone penetration tests (SCPT), which were performed at three different locations across the site (see Figure 1). The results of these in-situ measurements are reported in Figure 9d in terms of normalised initial stiffness (G_0/σ'_{v0}) profiles, together with cross-hole data reported by Hashash and Whittle (1996) for a South Boston site. The same figure shows the different stiffness profiles adopted in the FE simulations. For the M1 and M2 analyses, the low values of G_0 with depth, which are significantly smaller than those measured in-situ, were obtained from the calibrated parameter κ^* reported in Table 4. This limitation of hypoelastic models justifies the use of the Viggiani and Atkinson elastic model in the M3 and M4 analyses to capture the small-strain elastic stiffness of the soil deposit. In these cases, the stiffness parameters *A*, *m* and *n*, equal to 1600, 0.22 and 0.76, respectively, were selected based on the average PI of BBC (i.e. 20%). The corresponding normalised stiffness profiles match well both the in-situ data from SCPT tests and the measurements from other Boston sites (e.g. Hashash and Whittle, 1996).

Results and discussion

This section presents the results from the FE simulations, classified as indicated in Table 3. A sensitivity analysis to investigate the influence of the used constitutive models, as well as the influence of the two adopted elastic formulations on wall movements and surface settlements is provided.

Horizontal wall movements

Figures 10, 11 and 12 present the horizontal wall movements of the retaining structure in Section A predicted after excavation phases 1, 3 and 5, respectively. The available field measurements for the different excavation levels are also plotted on the same figures. The deflected profiles of the wall in Section B are shown in Figures 13, 14 and 15 for excavation phases 1, 3 and 5, respectively, together with the measured data. The field measurements shown in these figures were obtained from inclinometers embedded within the wall at the two locations (Chartier *et al*., 2010).

In general, the results show that FE analyses employing the traditional elasticity law (i.e. M1 and M2) generate larger wall deflections during all stages of the excavation process. In terms of comparison with measured displacements, these FE analyses employing the conventional elasticity law significantly overestimate the wall deflections for all excavation stages.

The flexibility of the SPTC adopted in Section B relative to the reinforced concrete wall used in Section A is evident by the difference in the deflected shape of Section B, where a sharper curvature is observed. The simulations suggest that the top-of-wall movement for the SPTC retaining structure is significantly limited by the top tieback, an observation which has also been made during the monitoring process on site. However, the analyses generally overestimate the wall pull-back upon initial application of the pre-stress for Section A which consequently influence the deflections at the top of the wall during excavation. During the first excavation phase (under cantilever conditions), the wall in Section A exhibits larger deflection than Section B. This is attributed to the greater depth of excavation at Section A for this stage (approximately 2.60 m deeper than at Section B).

With respect to a standard MCC analysis (M1), the introduction of the bubble allows for progressive yielding of the clay and invokes plastic deformations from the initial stages of loading. For both sections, the results obtained with a M2 analysis are very similar to those of M1 simulations during the first excavation phase mainly due to the fact that this phase included excavation in the made ground and fluvial sand layers only. The subsequent excavation phases, however, involve the BBC layer and the application of the bubble model results in increased wall deflections for both retaining systems compared to MCC simulations.

Once the Viggiani and Atkinson formulation for the small-strain stiffness was adopted (M3) and the initial degree of structure was also included in the simulations (M4), the numerical predictions are strongly influenced by the elastic response, irrespective of the type of retaining system. With respect to the M2 simulation, the maximum wall deflection for Section A exhibits a reduction of 54% from almost 6.0 cm to 2.7 cm at the final level of excavation for the M3 analysis. The reduction of the wall deflections in Section B is of similar order to Section A (approximately 58%) when the alternative elasticity formulation is employed (M3). This noteworthy difference can be attributed to the high initial stiffness at small strains predicted with the Viggiani and Atkinson model, a feature which cannot be attained by the traditional elasticity law (see Figure 9d), unless unrealistic values for the compressibility parameter κ^* are used in M1 and M2 analyses. The soil interacting with the excavation produces subtle differences in the numerical predictions between M3 and M4 analyses. This is attributed to the fact that the investigated problem is driven by small-strain non-linearity and the presence of an initial structure in the M4 analysis modifies only marginally the predictions. The post peak softening described by the KHSM results in a small increase of the simulated wall deflections for the two types of retaining structures, with a difference between the predictions of M3 and M4 analyses equal to approximately 10% in Section A and 8% in Section B. At excavation level 1, the M3 and M4 predictions are in good agreement with the measured wall deflections for Section A (Figure 10). On the contrary, the M3 and M4 analyses for Section B underestimate the maximum wall deflection by 0.20 cm (Figure 13). The advanced FE predictions are also in fair agreement with measured lateral soil deformations at excavation level 3

(Figures 11 and 14) and after the last excavation phase (Figures 12 and 15). The toe and maximum wall deflections are well captured by the M3 and M4 simulations, although the top-of-wall deflection is somehow underestimated. This could be explained by the reported disturbance caused by the use of pressurized drilling fluid with external flush and pressured grout without packers. It was in fact reported (Buro Happold, 2007) that this process may have caused hydraulic fracturing of the cohesive soils retained by the excavation walls.

Surface settlements

In view of the actual site geology, ground model and proposed depth, a horizontal extent of ground movement in the range of 2.5 to 4.0 times the depth of excavation was anticipated (as suggested by Peck, 1969).

The ground settlement profiles actually predicted by the four types of numerical analyses are presented in Figures 10, 11 and 12 for Section A and Figures 13, 14 and 15 for Section B at three excavation stages. Consistently with previous observations in terms of wall horizontal displacements, the maximum settlement predicted by the analyses employing the conventional elasticity model (i.e. M1 and M2) always exceeds those predicted by the Viggiani and Atkinson model (M3 and M4) for both sections at the three excavation levels presented. The differences between the M3 bubble model simulations and the KHSM analyses (M4) are, instead, always negligible. Comparing Figures 10 and 13, the Soldier Pile Tremie Concrete Wall used in Section B exhibits considerably smaller vertical settlements, since the first excavation level is significantly shallower (0.3 m below ground level). For all the other excavation stages, the difference between the settlements recorded behind the two wall is negligible. Finally, settlement results for Sections A and B are represented in Figures 16a and 16b with normalised vertical settlement, δ_v/δ_{vmax}, plotted against normalised wall depth (i.e. wall depth divided by maximum excavation depth, H_e). They are compared with the non-dimensional settlement envelopes proposed by Clough and O'Rourke (1990), reported on the same figure. The maximum settlement does not occur at the wall, as it would typically happen in stiff clays, but at some distance from the retaining system with the

displacements extending to more than $4H_e$. The troughs predicted by all four types of analyses in both sections somehow resemble the behaviour observed on several case histories for soft to medium clays, although they extend more than what suggested by observations. The normalised maximum vertical settlements are about 0.20% of H_e and are in good agreement with the range of 0.01% and 0.2% reported by Long (2001) for retaining walls in stiff clays with a large safety factor against excavation base heave. The predicted settlements are also in good agreement with the limiting value of 0.3% given by Clough and O'Rourke (1990) in the vicinity of the wall.

Time dependent behaviour of the excavation

The time dependent behaviour of the excavation was analysed in order to evaluate the performance of the KHSM. During excavation processes in saturated clayey soils, an accumulation of negative pore water pressures in the soil below the excavation base is observed. The assessment of time and movement dependent uplift soil pressure due to the generation of negative excess pore water pressures at the excavation base is a typical finite element soil-structure interaction problem. Based on the results from the previous sections, only the KHSM was considered in this part of the work and the retaining system adopted for Section B was analysed. The monitoring system, composed by vibrating wire piezometers (PZ) and magnetic extensometers (EXT), was used to measure pore water generation and dissipation with time, as well as movements of the excavation base. In particular, the piezometers PZ4-1, PZ4-2 and PZ4-3, located respectively at 17 m, 22 m and 31m from ground surface below the excavation, and the extensometers EXT 02-8, EXT 02-6 and EXT 02-3, approximately at the same depths below ground level, were considered (Figure 4). A coupled-consolidation analysis was performed in order to replicate as close as possible the excavation sequence of this section of the retaining system. The FE simulations used an isotropic value of permeability equal to 3.00×10^{-10} m/s for the BBC and glacial till layers, evaluated from the self-boring pressuremeter and CRSC tests (Figure 2c), and 1.50×10^{-5} m/s for the made ground and fluvial sands strata. Impermeable boundaries were imposed at the base and along the lateral sides of the mesh while free boundaries were imposed at ground surface behind and in front of the wall. The

retaining structure was simulated as an impermeable material. Figure 17a reports the time history of the excavation process, while Figures 17b and 17c show the measured and predicted time histories of pore pressures and heave movements beneath the centre of the excavation. It can be noted that the numerical analysis is able to accurately capture both the pore water pressure changes with time due to the unloading phase and the associated heave of the excavation base at the three investigated depths.

Conclusion

The paper examined the undrained behaviour of a deep excavation which forms part of a 100 m wide basement excavation located in Boston, Massachusetts, USA. Two different types of tied back retaining walls were used, a soldier pile tremie concrete wall and a traditional reinforced concrete diaphragm wall. The glacial marine clay foundation was modelled with the Kinematic Hardening Model for Structured soils (KHSM), its reduced bubble model version (KHM) and the MCC model along with a traditional elasticity and a small-strain stiffness formulation. Also, the pore pressure time histories beneath the centre of the excavation and the associated heave of its base were modelled with coupled finite element analyses.

A calibration procedure of the constitutive model parameters was conducted based on various sources of experimental data. The calibrated parameters were evaluated by means of numerical simulations of undrained triaxial, constant rate of strain and self-boring pressuremeter tests. The values for the OCR profile were carefully selected in order to closely reproduce the design profile of undrained shear strength.

The FE analyses revealed that the numerical simulations using the kinematic hardening models provide a close match to field monitoring data. The analyses employing the Viggiani and Atkinson formulation for the small-strain stiffness indicated that the numerical predictions are strongly influenced by the elastic formulation adopted in the constitutive model, irrespective of the type of retaining system, with wall deflection reducing to approximately half for both retaining systems. This significant change in the predictions is attributed to the high initial stiffness at small strains, a

feature which cannot be attained by the traditional elasticity law, unless unrealistic elastic parameters are adopted. Introducing structure degradation in this study offered only a relatively small increase in the wall deflections, which can be attributed to the post peak softening behaviour accounted for in the KHSM.

Finally, the work examined the time dependent behaviour of the excavation by means of coupled-consolidation analyses replicating the actual construction timeline. The KHSM was very successful in predicting the magnitude and rate of change of pore water pressure and the base heave induced by the excavation.

Acknowledgments

The third author would like to acknowledge the financial support provided by EPSRC and Buro Happold Ltd during his doctoral programme. We are also grateful to the anonymous reviewers for their valuable comments and suggestions.

References

Addenbrooke T.I., Potts D.M., Puzrin A.M. (1997). The influence of pre-failure soil stiffness on the numerical analysis of tunnel construction. Géotechnique, 47(3):693-712.

Berman D.R., Germaine J.T., Ladd C.C. (1993). Characterization of engineering properties of Boston Blue Clay for the MIT campus. Research Report 93-16, MIT, Cambridge, MA, 146p.

Burland J.B. (1990). On the compressibility and shear strength of natural clays. Géotechnique, 40(3):329-378.

Burland J.B. and Hancock R.J.R. (1977). Underground car park at the House of Commons, London. The Structural Engineer, 55:87-100.

Buro Happold (2007). Harvard Allston Science Complex. Geotechnical Report – Rev.4. Buro Happold Limited.

Chang C.Y. and Duncan J.M. (1970). Analysis of soil movement around a deep excavation. Proc. ASCE, 96(SM5):1655-1970.

Chartier M., Nikolic A., Fasano A., Sun R.Y.F. (2010). Observed performance of two anchored retaining wall systems for an excavation in Boston. Proc. Int. Geotech. Conf., Geotechnical Challenges in Megacities, Moscow, Vol. 2, 585-592.

Clough G.W. and O'Rourke T.D. (1990). Construction induced movements of in situ walls. Proc. Conf. on Design and Performance of Earth Retaining Structures, ASCE Special Publication, 15, 439-470.

Cotecchia F. and Chandler R.J. (2000). A general framework for the mechanical behaviour of clay. Géotechnique, 50(4):431-447.

Elia G. and Rouainia M. (2013a). Seismic performance of earth embankment using simple and advanced numerical approaches. J. Geotech. Geoenv. Eng. ASCE, 139(7):1115-1129.

Elia G. and Rouainia M. (2013b). Performance evaluation of a shallow foundation built on structured clays under seismic loading. Bulletin of Earthquake Engineering, 12(4):1537-1561.

Fayad P. (1986). Aspects of the volumetric and undrained shear behavior of Boston Blue Clay. S.M. Thesis, MIT, Cambridge, MA.

Gonzáles N.A., Rouainia M., Arroyo M., Gens A. (2012). Analysis of tunnel excavation in London Clay incorporating soil structure. Géotechnique, 62(12):1095-1109.

Hashash Y.M.A. and Whittle A.J. (1996). Ground movement prediction for deep excavations in soft clay. J. Geotech. Eng. ASCE, 122(6):474-486.

Kung G.T.C., Ou C.Y., Juang C.H. (2009). Modelling small-strain behaviour of Taipei clays for finite element analysis of braced excavations. Computers and Geotechnics, 36(1-2):304-319.

Ladd C.C., Young G.A., Kramer S.A., Burke D.M. (1999). Engineering properties of Boston Blue Clay from special testing program. Proc. ASCE Geo-Congress 98, GSP(91), 1-24.

Ladd C.C. and Varallyay J. (1965). The influence of stress system on the behaviour of saturated clays during undrained shear. Report No 1, part II, Report R65-11, MIT, Cambridge, MA, 263p.

Long M. (2001). Database for retaining wall and ground movements due to deep excavations. J. Geotech. Geoenv. Eng. ASCE, 127(3):203-224.

Nikolic A., Fasano A., Cook J. (2010). Undrained shear strength evaluation for natural Boston Blue Clay. Proc. DFI (Deep Foundation Institute) Conference on Geotechnical Challenges in Urban Regeneration, London (UK).

Nikolinakou M.A., Whittle A.J., Savidis S., Schran U. (2011). Prediction and interpretation of the performance of a deep excavation in Berlin Sand. J. Geotech. Geoenv. Eng. ASCE, 137(11):1047-1061.

O'Rourke T.D. and O'Donnell C.J. (1997). Field behavior of excavation stabilized by deep soil mixing. J. Geotech. Geoenv. Eng. ASCE, 123(6):516-524.

Panayides S., Rouainia M., Muir Wood D. (2012). Influence of degradation of structure on the behaviour of a full-scale embankment. Can. Geotech. J., 49:344-356.

Peck R.B. (1969). Deep excavations and tunnelling in soft ground. Proc. 7th Int. Conf. Soil Mech., Mexico, 225-290.

PLAXIS 2D (2012). Reference Manual. Plaxis bv, P.O. Box 572, 2600 AN Delft, The Netherlands.

Powrie W. and Batten M. (2000). Comparison of measured and calculated temporary proploads at Canada Water Station. Géotechnique, 50(2):127-140.

Puller M. (2003). Deep Excavations: a practical manual (2nd Edition). Thomas Telford, London.

Rouainia M. and Muir Wood D. (2000). A kinematic hardening model for natural clays with loss of structure, Géotechnique, 50(2):153-164.

Santagata M.C. (1998). Factors affecting the initial stiffness and the stiffness degradation behavior of cohesive soils. Ph.D. Thesis, MIT, Cambridge, MA.

Santagata M.C. and Germaine J.T. (2002). Sampling disturbance effects in normally consolidated clays. J. Geotech. Geoenv. Eng. ASCE, 128(12):997-1006.

Santagata M.C., Germaine J.T., Ladd C.C. (2005). Factors affecting the initial stiffness of cohesive soils. J. Geotech. Geoenv. Eng. ASCE, 131(4):430-441.

Sheahan T.C. (1991). An experimental study of the time-dependent undrained shear behaviour of resedimented clay using automated stress path triaxial equipment. Sc.D. Thesis, MIT, Cambridge, MA.

Simpson B., O'Riordan N.J., Croft D.D. (1979). A computer model for the analysis of ground movements in London Clay. Géotechnique, 29(2):149-175.

Terzaghi K., Peck R.B., Mesri G. (1996). Soil Mechanics in Engineering Practice (3rd Edition). John Wiley & Sons, New York.

Viggiani G. and Atkinson J.H. (1995). Stiffness of fine-grained soils at very small strains. Géotechnique, 45(2):249-265.

Whittle A.J., Hashash Y.M.A., Whitman R.V. (1993). Analysis of deep excavation in Boston. J. Geotech. Eng. ASCE, 119(1):69-90.

Whittle A.J., Corral G., Jen L.C., Rawnsley R.P. (2015). Prediction and performance of deep excavations for Courthouse Station, Boston. J. Geotech. Geoenv. Eng. ASCE, 141(4):04014123.

Zdravkovic L., Potts D.M., St John H.D. (2005). Modelling of a 3D excavation in finite element analysis. Géotechnique, 55(7):497-513.

Zhao J., Sheng D., Rouainia M., Sloan S.W. (2005). Explicit stress integration of complex soil models. Int. J. Num. Anal. Meth. Geomech., 29:1209-1229.

Appendix A: Constitutive model formulation

The mathematical formulation of the model in the general stress space is summarised in the following. Since the model describes the response of the soil skeleton, all stresses are effective stresses (the primes have been dropped for simplicity). The symbol ':' indicates a summation of products, the dots over symbols indicate an infinitesimal increment of the corresponding quantity, whereas bold-face symbols indicate tensors.

The expression of the reference surface is:

$$f_r = \frac{3}{2M_\theta^2}\boldsymbol{s}:\boldsymbol{s} + \left(p - p_c\right)^2 - \left(p_c\right)^2 = 0 \tag{1}$$

The bubble surface is written as:

$$f_b = \frac{3}{2M_\theta^2}\left(\boldsymbol{s} - \boldsymbol{s}_{\bar{\alpha}}\right):\left(\boldsymbol{s} - \boldsymbol{s}_{\bar{\alpha}}\right) + \left(p - p_{\bar{\alpha}}\right)^2 - \left(Rp_c\right)^2 = 0 \tag{2}$$

The structure surface is given by:

$$F = \frac{3}{2M_\theta^2}\left[\boldsymbol{s} - \left(r-1\right)\boldsymbol{\eta}_0 p_c\right]:\left[\boldsymbol{s} - \left(r-1\right)\boldsymbol{\eta}_0 p_c\right] + \left(p - rp_c\right)^2 - \left(rp_c\right)^2 = 0 \tag{3}$$

where p_c is the effective stress which defines the size of the reference surface, R is the size of the bubble, $\boldsymbol{\eta}_0$ a deviatoric tensor controlling the structure, r is the ratio of the sizes of the structure and the reference surfaces, p and $\boldsymbol{s}$ are the mean pressure and deviatoric stress tensor. The dimensionless scaling function, M_θ, for deviatoric variation of the critical state stress ratio with the Lode angle θ, is defined by:

$$M_\theta = M\left[\frac{2\alpha^4}{1+\alpha^4-(1-\alpha^4)\sin(3\theta)}\right]^{1/4} \tag{4}$$

where M is the slope of the critical state line under triaxial compression ($\theta = -30^\circ$) and $\alpha = (3-\sin\phi')/(3+\sin\phi')$, with ϕ' being the internal friction angle.

The scalar variable *r*, which is a monotonically decreasing function of both plastic volumetric and shear strain, represents the progressive degradation of the material as follows:

$$\dot{r} = -\frac{k}{(\lambda^* - \kappa^*)}(r-1)\dot{\varepsilon}_d \tag{5}$$

where λ^* and κ^* are the slopes of normal compression and swelling lines in the ln*v* : ln*p* compression plane (being *v* the soil specific volume) and *k* is a parameter which controls the structure degradation with strain. The rate of the destructuration strain $\dot{\varepsilon}_d$ is assumed to have the following form:

$$\dot{\varepsilon}_d = \left[(1-A^*)\left(\dot{\varepsilon}_v^p\right)^2 + A^*\left(\dot{\varepsilon}_q^p\right)^2\right]^{1/2} \tag{6}$$

where A^* is a non-dimensional scaling parameter and $\dot{\varepsilon}_q^p$ and $\dot{\varepsilon}_v^p$ are the plastic shear and volumetric strain rate, respectively.

Volumetric hardening rule is adopted in the model, where the change in size of the reference surface, p_c, is controlled only by plastic volumetric strain rate, $\dot{\varepsilon}_v^p$, given by:

$$\frac{\dot{p}_c}{p_c} = \frac{\dot{\varepsilon}_v^p}{\lambda^* - \kappa^*} \tag{7}$$

If a stress increment requires movement of the bubble relative to the structure surface, the following kinematic hardening is invoked:

$$\dot{\boldsymbol{\alpha}} = \dot{\hat{\boldsymbol{\alpha}}} + \frac{\dot{p}_c}{p_c}(\bar{\boldsymbol{\alpha}} - \hat{\boldsymbol{\alpha}}) + \dot{\mu}(\boldsymbol{\sigma}_c - \boldsymbol{\sigma}) \tag{8}$$

where $\bar{\boldsymbol{\alpha}}$ and $\hat{\boldsymbol{\alpha}} = p_c\left[r\boldsymbol{I} + (r-1)\boldsymbol{\eta}_0\right]$ denote the locations of the centre of the bubble and structure surface respectively, $\boldsymbol{\sigma}_c$ is the conjugate stress and μ is a positive scalar of proportionality. It should be noted that the centre of the structure surface and the deviator of $\hat{\boldsymbol{\alpha}}$ represents the anisotropy of the soil due to structure. The deviator of $\hat{\boldsymbol{\alpha}}$ therefore degrades to zero as *r* degrades to unity.

The plastic modulus *H* is assumed to depend on the distance between the current stress and the conjugate stress and is given by:

$$H = H_c + \frac{Bp_c^3}{(\lambda^* - \kappa^*)R}\left(\frac{b}{b_{\max}}\right)^{\psi} \tag{9}$$

where H_c is the plastic modulus at the conjugate stress, *B* and ψ are two additional material properties, $b = \bar{\boldsymbol{n}} : (\boldsymbol{\sigma}_c - \boldsymbol{\sigma})$ is the normalised distance between the bubble and the structure surface and $b_{\max} = 2(r/R - 1)\bar{\boldsymbol{n}} : (\boldsymbol{\sigma} - \bar{\boldsymbol{\alpha}})$ is its maximum value.

Finally, a classical hypoelastic formulation, accounting for a linear dependence of both bulk and shear moduli on mean effective pressure, can be adopted in the model. Alternatively, the well-known equation proposed by Viggiani and Atkinson (1995) for the small-strain shear modulus (G_0) can be used:

$$\frac{G_0}{p_r} = A\left(\frac{p}{p_r}\right)^n R_0{}^m \tag{10}$$

where A, m and n are dimensionless stiffness parameters, p_r is a reference pressure (equal to 1 kPa), p is the mean effective stress and $R_0 = 2p_c/p$ is the isotropic overconsolidation ratio.

Notation

A, m, n	non-dimensional factors in Equation (10)
b	normalised distance between bubble and structure surface
b_{max}	maximum value of b
c_u	undrained shear strength
E_u	undrained secant modulus
F	structure yield surface
f_r	reference yield surface
f_b	bubble yield surface
G_0	small-strain shear modulus
H	plastic modulus
H_c	plastic modulus at conjugate stress
$\boldsymbol{I}$	second rank identity tensor
K_0	at-rest earth pressure coefficient
$\bar{\boldsymbol{n}}$	normalised stress gradient on the bubble
OCR	overconsolidation ratio
p, p_0	mean effective stress
p_c	stress variable controlling size of the surfaces
q	scalar deviator stress
r	parameter describing ratio of sizes of structure and reference surfaces
$\mathbf{s}$	tensorial deviator stress
$\bar{\boldsymbol{\alpha}}$	location of the centre of the bubble
$\hat{\boldsymbol{\alpha}}$	location of the centre of the structure surface
ε_a	axial strain
ε_v	volumetric strain
ε_v^p	volumetric strain
ε_q^p	deviatoric strain
ε_d	damage strain
γ_t	total unit weight
μ	positive scalar of proportionality
$\boldsymbol{\sigma}$	effective stress tensor
$\boldsymbol{\sigma}_c$	conjugate stress
$\boldsymbol{\sigma}_v'$	vertical effective stress

Strata	Thickness (m)	Description
Made ground	1.2 – 2.7	Granular silty sand fill with fragments of gravel, concrete, clay, brick, ash and wood
Fluvial sands and gravels	2.1 –5.5	Medium dense to very dense sands and gravels
Boston Blue Clay	23.8 – 36.5	Stiff olive grey clay with occasional discontinuous sand and silt partings, becoming softer with depth
Glacial Till	1.5 – 6.4	Very dense grey silty, clayey sand with gravels
Cambridge Argillite (Bedrock)	encountered at 33.8 – 45.7	Medium to moderately hard fresh to slightly weathered thinly bedded grey mudstone

Table 1. Strata encountered during site investigations at the Harvard Allston Science Complex site

(Buro Happold, 2007)

Strata	c' (kPa)	ϕ' (°)	Unit weight (kN/m^3)	E' (MPa)	K_0	Poisson's ratio
Made ground – L_1	0.0	30	19.0	29	0.5	0.2
Fluvial sands and gravels – L_2	0.0	35	19.0	75	0.43	0.2
Glacial Till – L_4	0.0	37	21.5	100	0.6	0.2

Table 2. Design soil properties for L_1, L_2 and L_4

Analysis name	Model adopted for the BBC deposit	Elastic formulation
M1	MCC	Hypoelasticity
M2	KHM	Hypoelasticity
M3	KHM	Viggiani & Atkinson
M4	KHSM	Viggiani & Atkinson

Table 3. Classification of FE analyses

Parameter/ symbol	Physical contribution/meaning	NC BBC	OC BBC
M	Critical state stress ratio for triaxial compression	1.11	1.11
λ^*	Slope of normal compression line in ln$v$-ln$p$ compression plane	0.028	0.028
κ^*	Slope of swelling line in ln$v$-ln$p$ compression plane	0.004	0.004
R	Ratio of size of bubble and reference surface	0.08	0.08
B	Stiffness interpolation parameter	2.0	2.0
ψ	Stiffness interpolation exponent	1.35	1.35
η_0	Anisotropy of initial structure	**0.5**	**0.3**
r_0	Initial degree of structure	1.8	1.5
A^*	Parameter controlling relative proportion of distorsional and volumetric destructuration	0.5	0.5
k	Parameter controlling rate of loss of structure with damage strain	1.5	1.0
ν	Poisson's ratio	0.25	0.25

Table 4. KHSM parameters for L_3

Section name	Model	EA (kN/m)	EI (kNm^2/m)	Unit weight (kN/m^3)	Poisson's ratio
Section A	Elastic	2.28×10^7	1.59×10^6	22	0.2
Section B	Elastic	2.13×10^7	1.03×10^6	22	0.15

Table 5. Parameters adopted for the two retaining systems

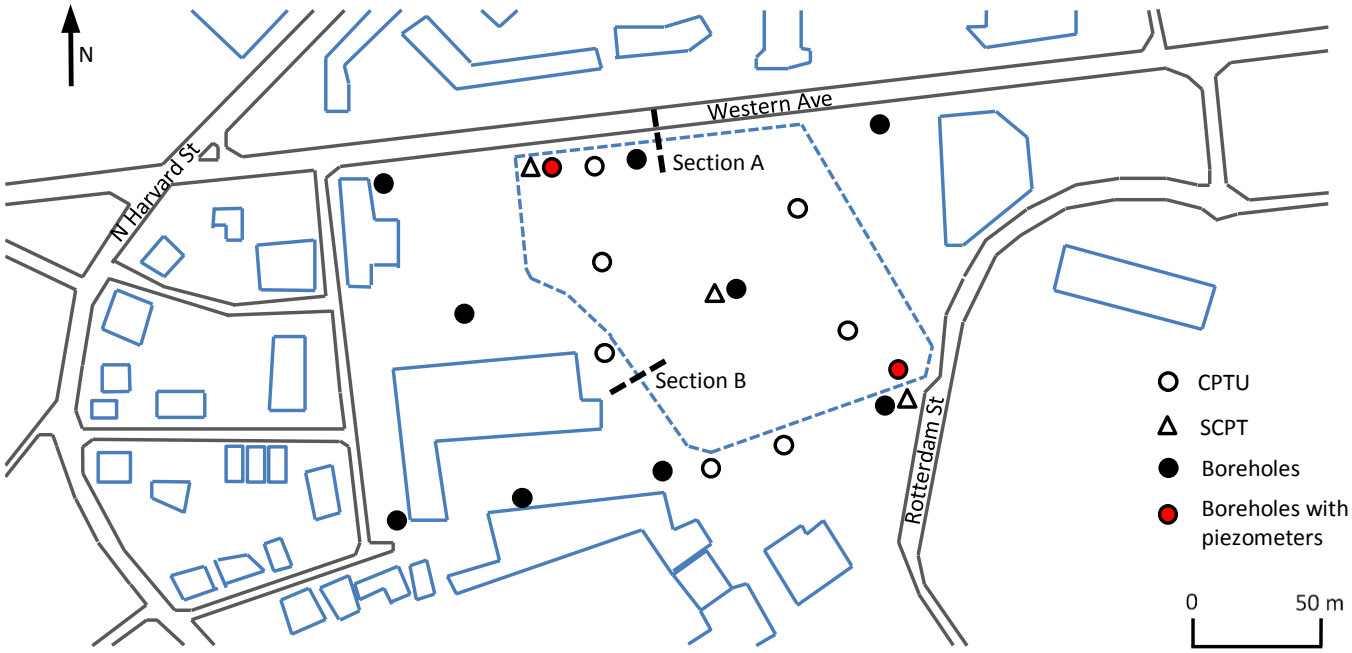


Figure 1. Allston Science Complex, Boston, USA and location of in-situ tests

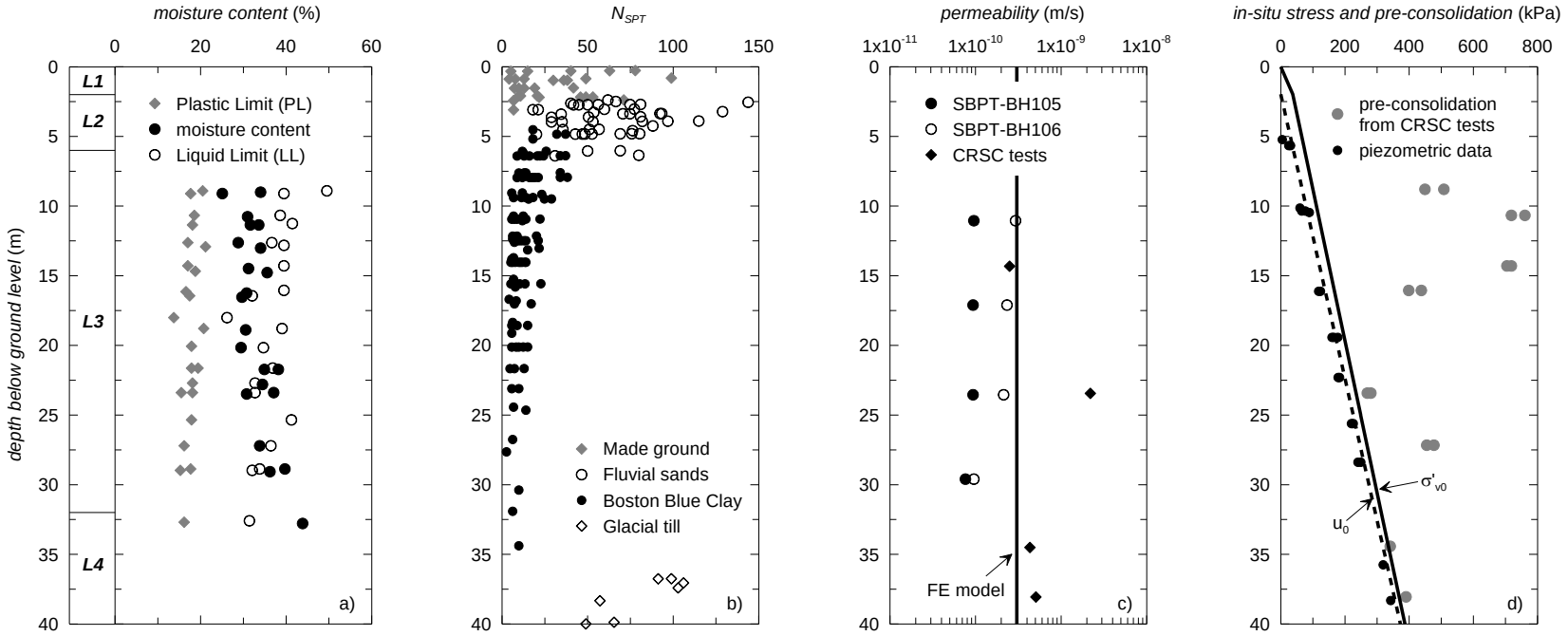


Figure 2. In-situ stresses and properties of BBC: a) moisture content; b) N_{SPT} data; c) permeability data; d) stress history

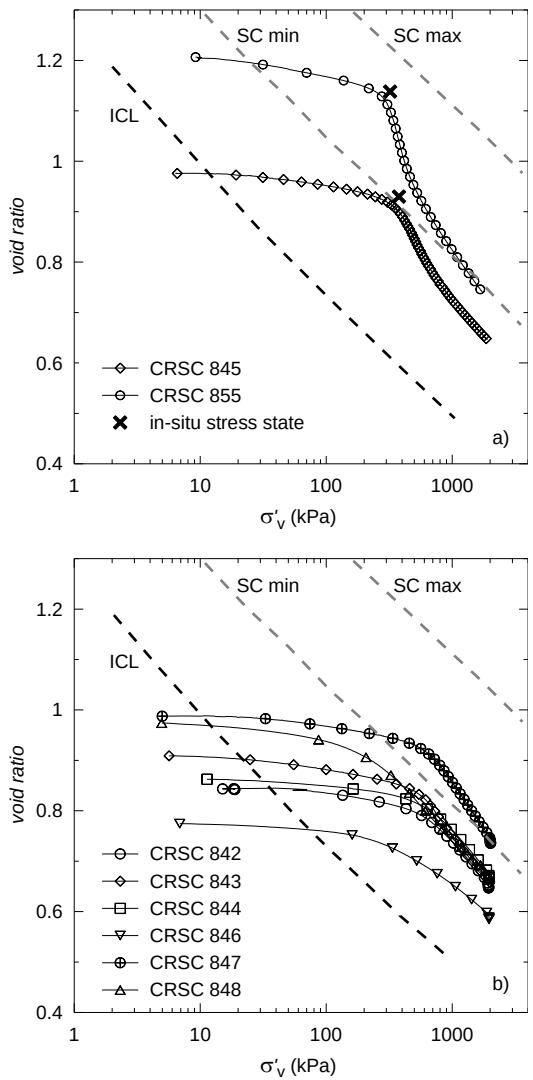
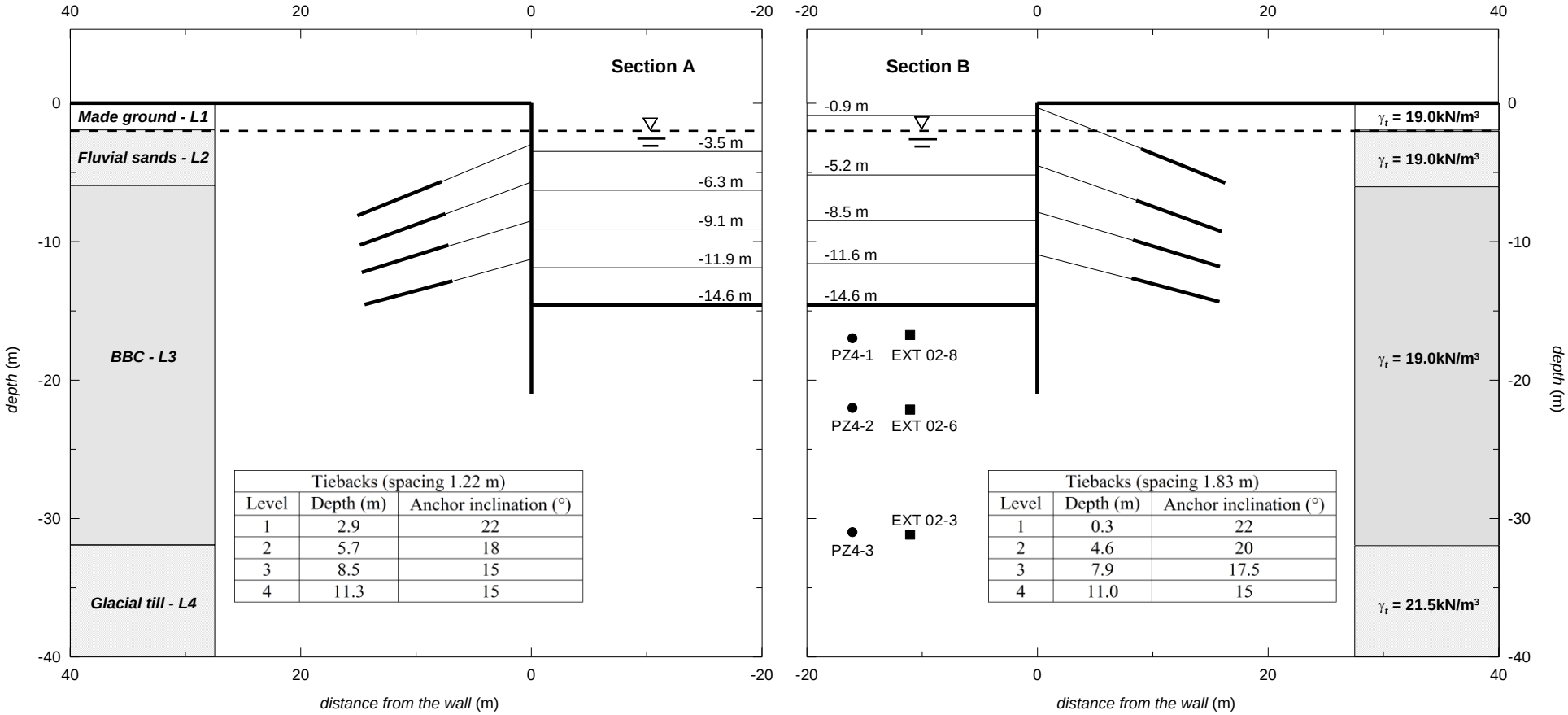


Figure 3. Results from CRSC tests on: a) natural NC BBC; b) natural OC BBC (adapted from Nikolic *et al.*, 2010)



Tiebacks (spacing 1.22 m)		
Level	Depth (m)	Anchor inclination (°)
1	2.9	22
2	5.7	18
3	8.5	15
4	11.3	15

Tiebacks (spacing 1.83 m)		
Level	Depth (m)	Anchor inclination (°)
1	0.3	22
2	4.6	20
3	7.9	17.5
4	11.0	15

Figure 4. Characteristics of the excavation support systems adopted in Section A and Section B

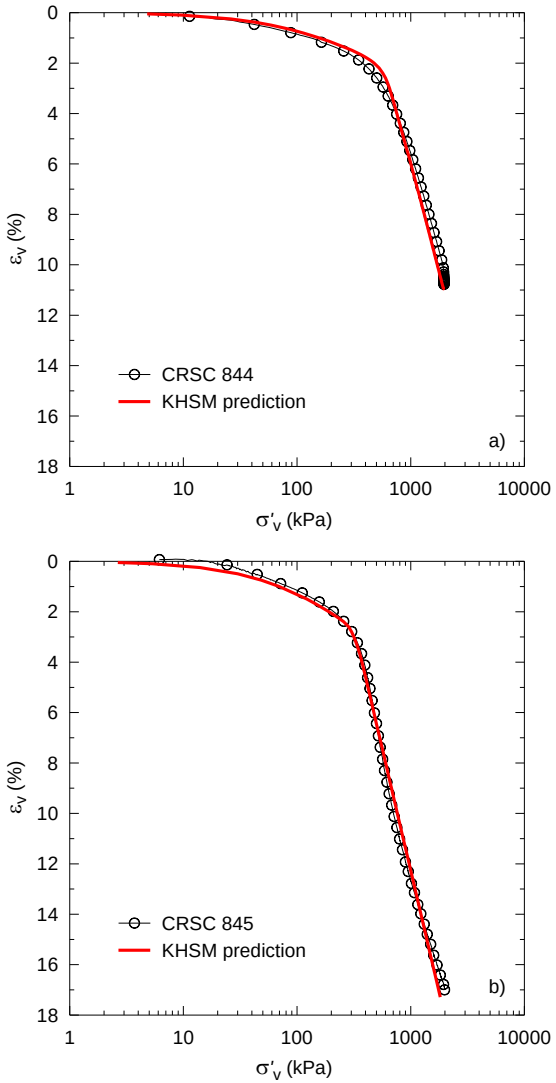


Figure 5. Comparison of KHSM predictions and CRSC tests on natural BBC samples: a) CRSC 844, depth 11m; b) CRSC 845, depth 38m

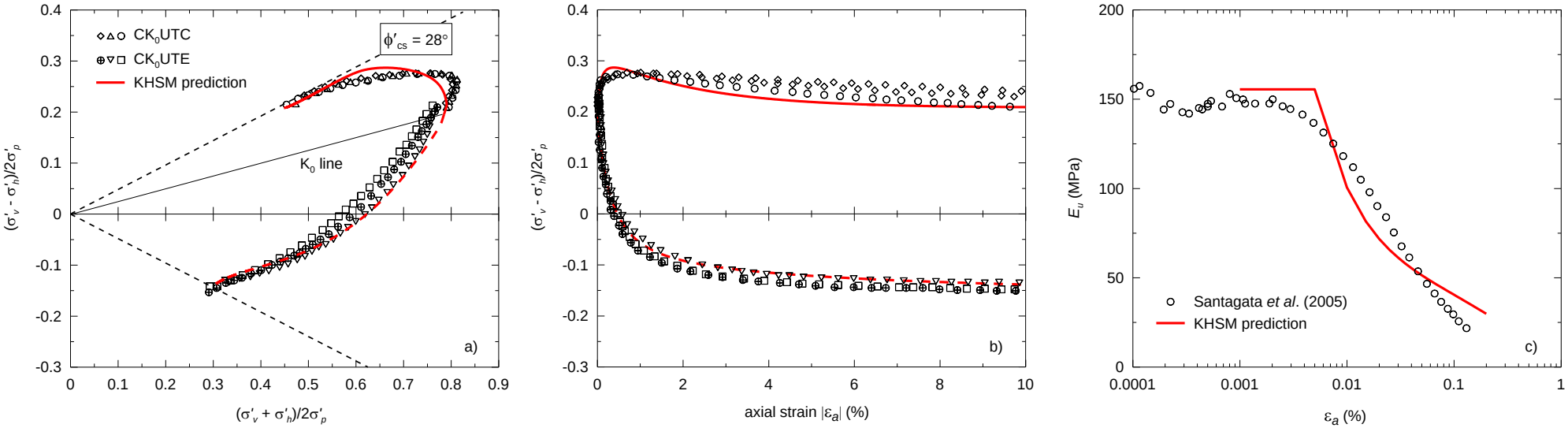


Figure 6. Comparison of KHSM predictions and undrained triaxial test results on anisotropically consolidated BBC: a) stress paths; b) stress-strain curves; c) undrained stiffness degradation curve

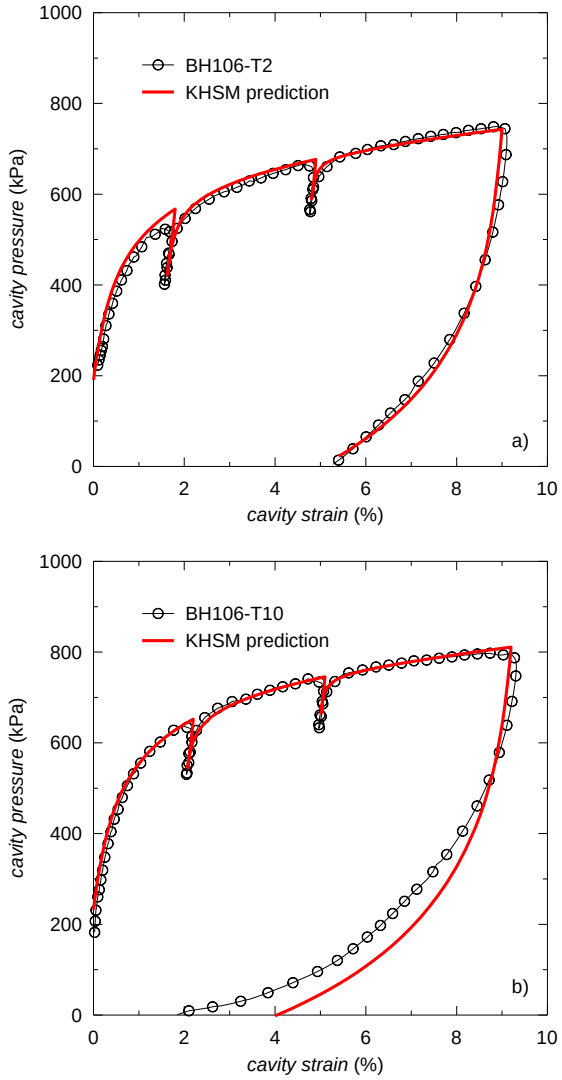


Figure 7. Comparison of KHSM predictions and self-boring pressuremeter tests on natural BBC samples: a) BH106-T2, depth 13m; b) BH106-T10, depth 35m

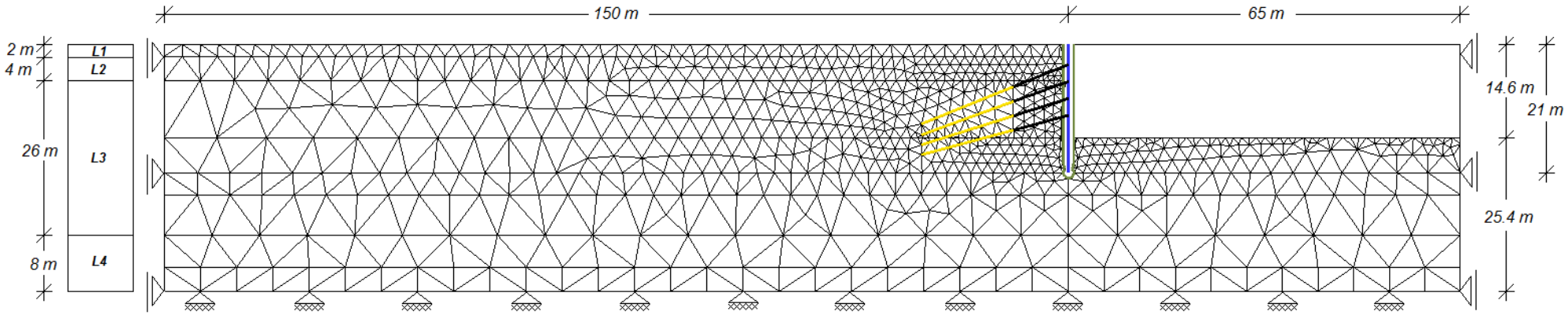


Figure 8. Geometry and finite element mesh of the excavation - Section A

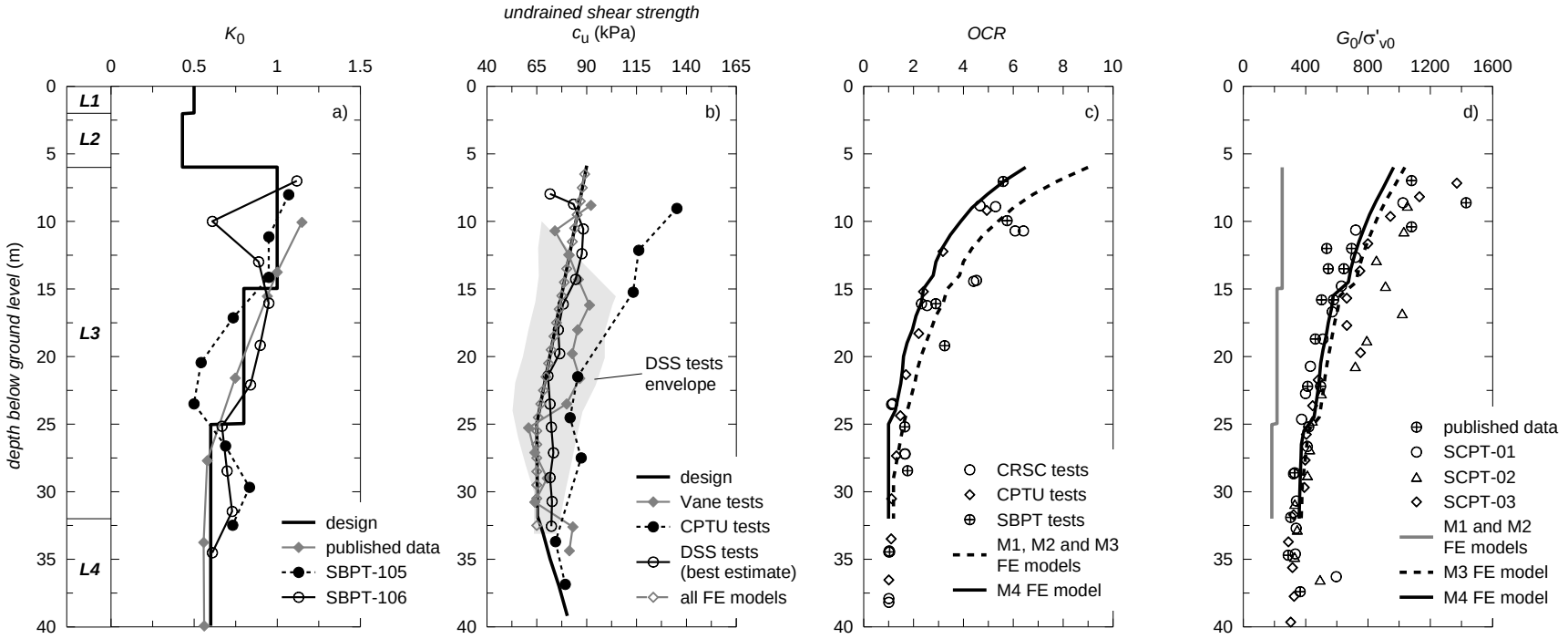


Figure 9. Comparison of numerical profiles with measured data at the Allston Science Complex: a) at-rest earth pressure coefficient; b) undrained shear strength; c) *OCR*; d) normalised G_0

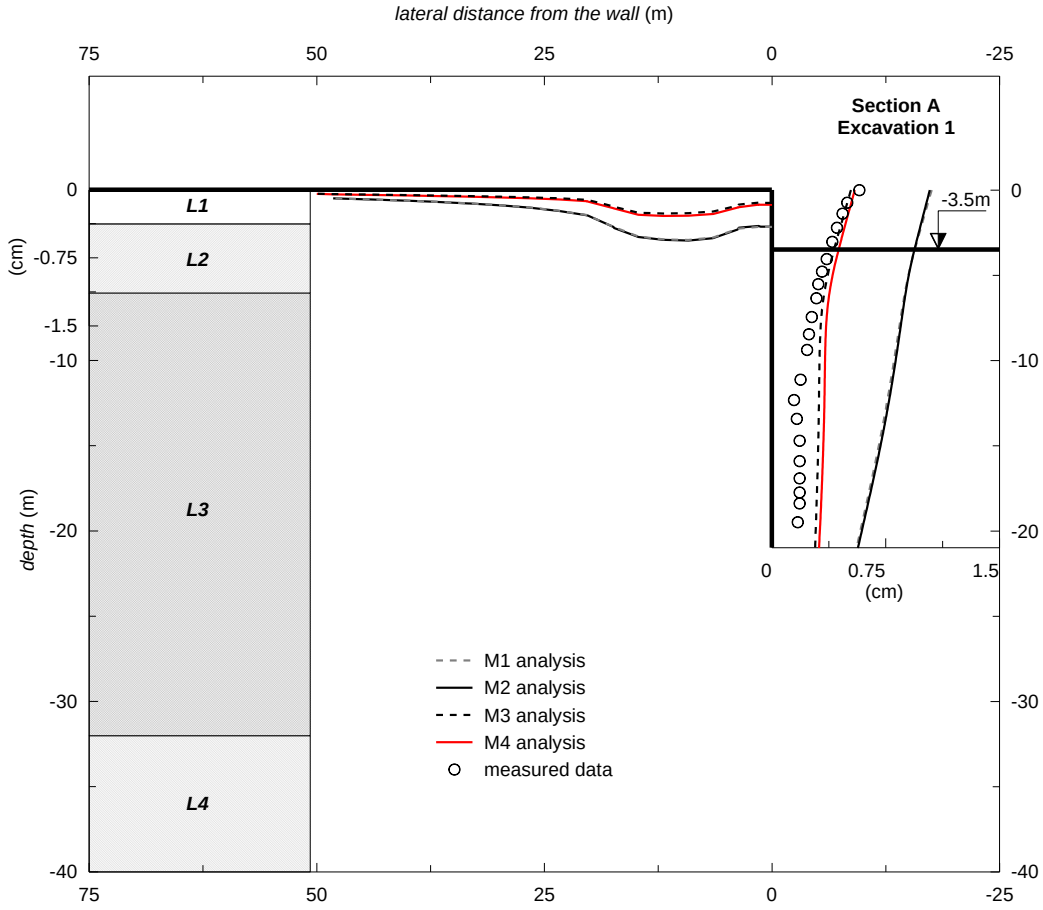


Figure 10. Predicted excavation performance (Section A - Excavation phase 1)

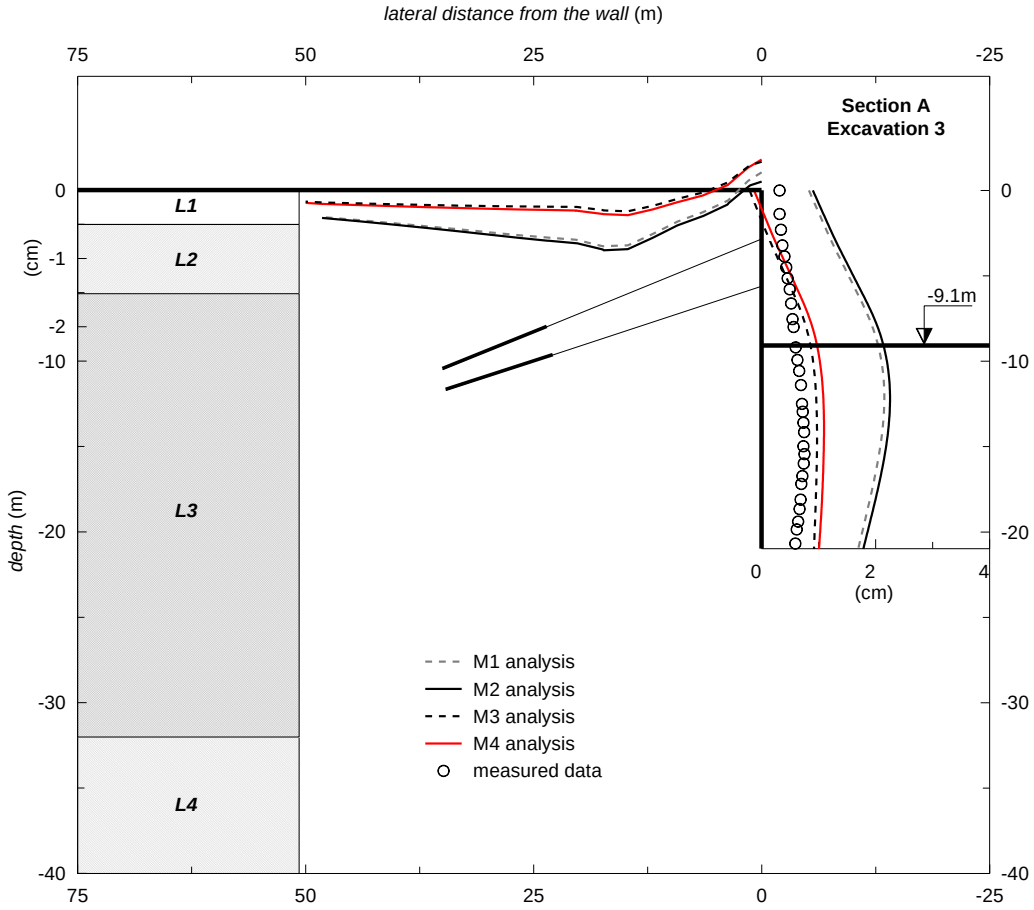


Figure 11. Predicted excavation performance (Section A - Excavation phase 3)

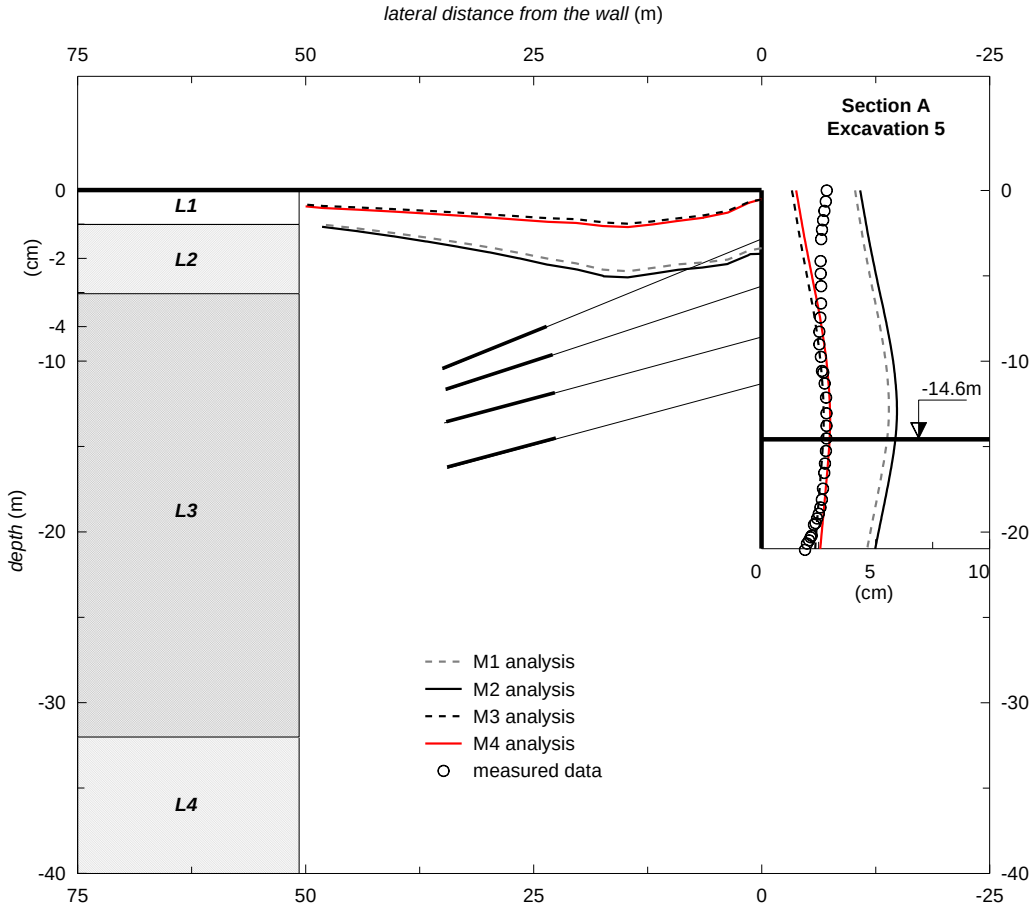


Figure 12. Predicted excavation performance (Section A - Excavation phase 5)

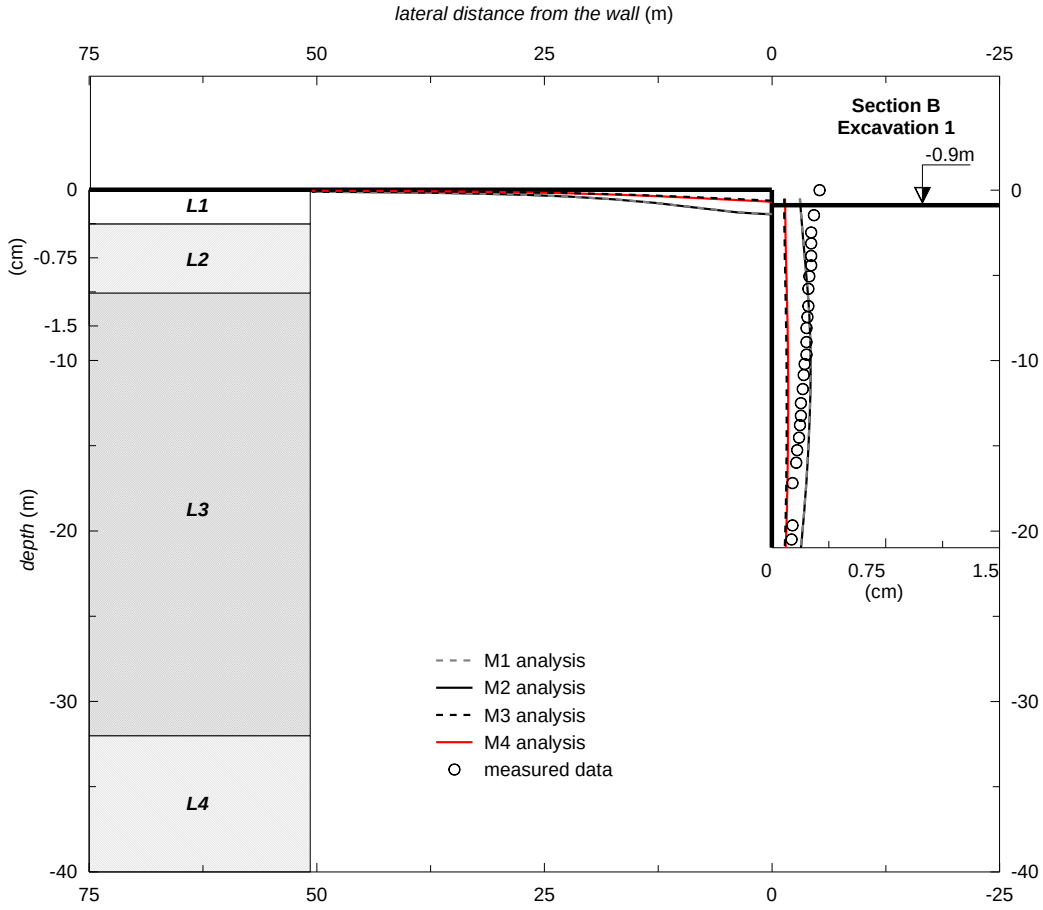


Figure 13. Predicted excavation performance (Section B - Excavation phase 1)

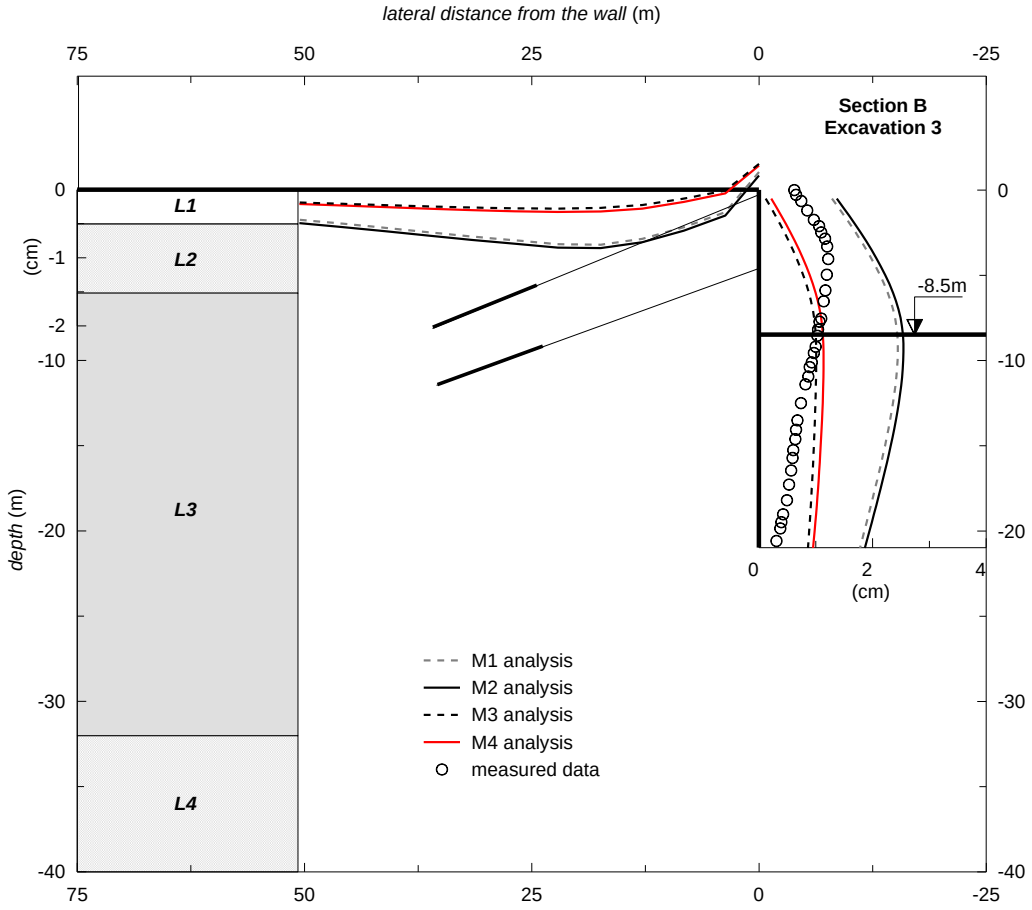


Figure 14. Predicted excavation performance (Section B - Excavation phase 3)

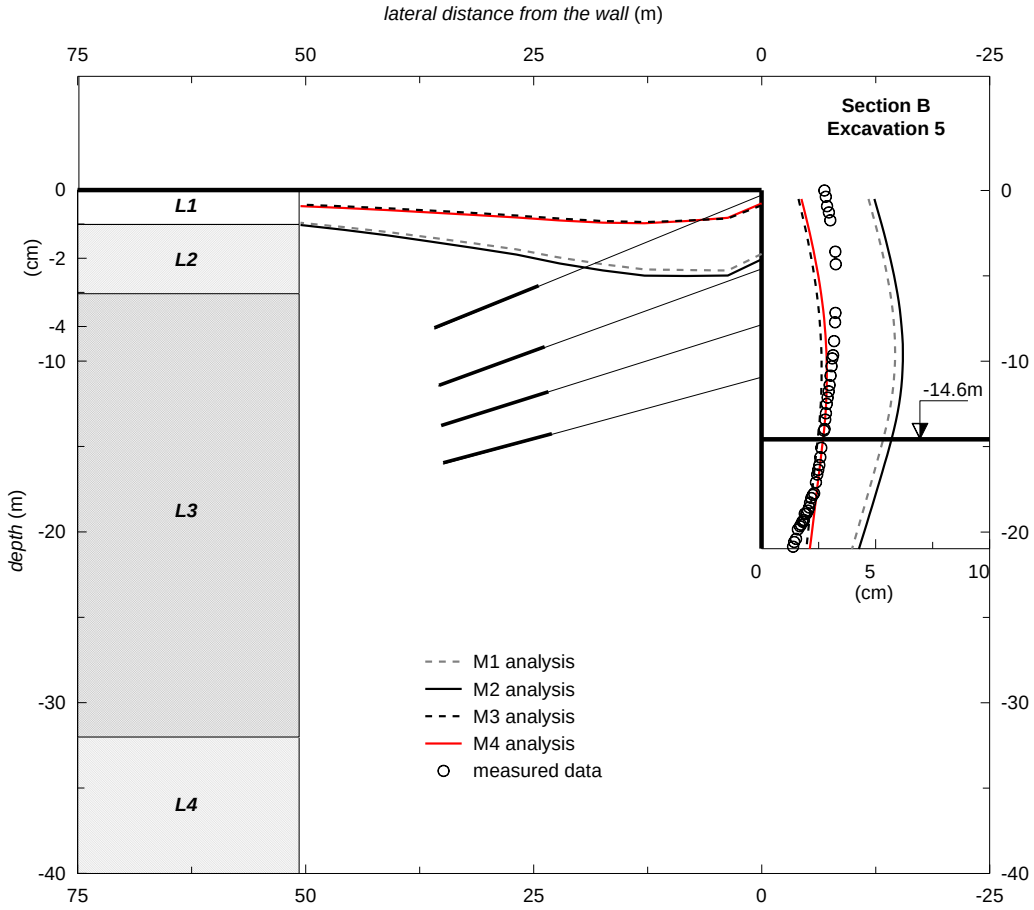


Figure 15. Predicted excavation performance (Section B - Excavation phase 5)

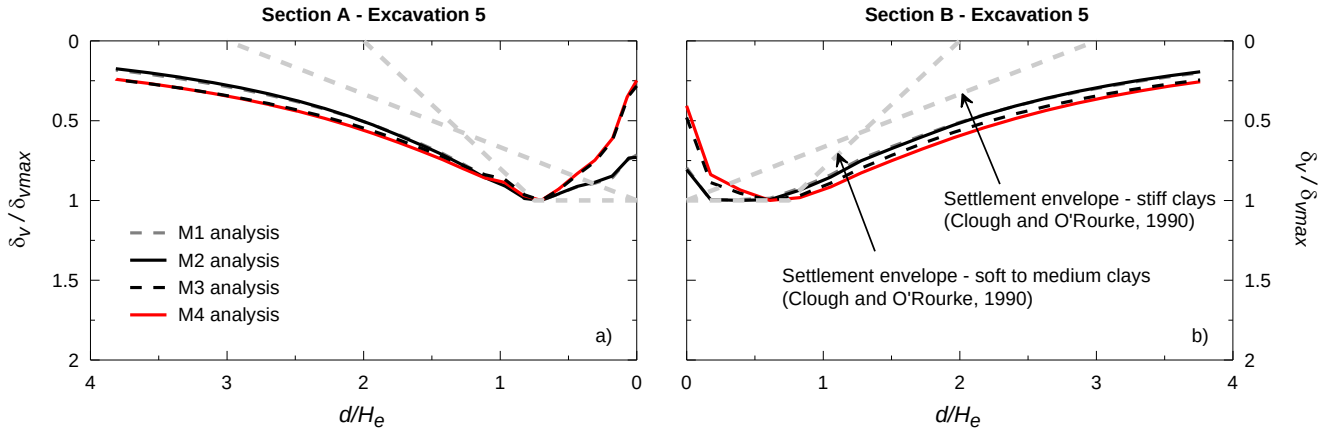


Figure 16. Normalised predicted settlements behind the wall at the end of Excavation 5: a) Section A; b) Section B

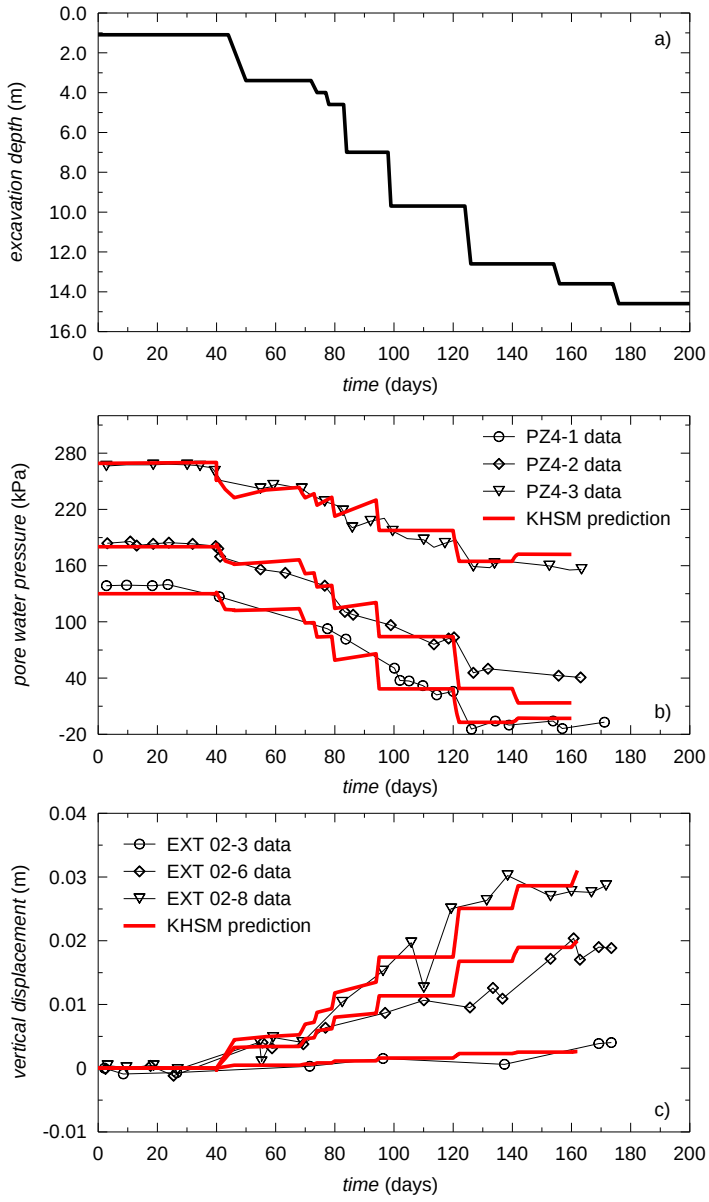


Figure 17. Consolidation analysis results: a) excavation stages; b) comparison of KHSM predictions with measured pore water pressures; c) comparison of KHSM predictions with magnetic extensometer ground movement measurements